On the Impact of Fixed Point Hardware for Optical Fiber Nonlinearity Compensation Algorithms

Tom Sherborne*, Benjamin Banks*, Daniel Semrau, *Student Member, IEEE*,
Robert I. Killey, *Senior Member, IEEE*, Polina Bayvel, *Fellow, IEEE*, and Domaniç Lavery, *Member, IEEE*

***Abstract*—Nonlinearity mitigation using digital signal processing has been shown to increase the achievable data rates of optical fiber transmission links. One especially effective technique is digital back propagation (DBP), an algorithm capable of simultaneously compensating for linear and nonlinear channel distortions. The most significant barrier to implementing this technique, however, is its high computational complexity. In order to fully characterize the performance of DBP, there is a need to model the algorithm under the constraint of a fixed hardware complexity which, crucially, would include the bit-depth of the multiplication operation. In this work, DBP and a single nonlinear step DBP implementation, the *Enhanced Split Step Fourier* method (ESSFM), are compared with linear equalization using a generic software model of fixed point hardware. The requirements of bit depth and fast Fourier transform (FFT) size are discussed to examine the optimal operating regimes for these two schemes of digital nonlinearity compensation. For a 1000 km transmission system, it was found that (assuming an optimized FFT size), in terms of SNR, the ESSFM algorithm outperformed the conventional DBP for all hardware resolutions up to 13 bits.**

***Index Terms*—Optical Fiber Communication, Digital Signal Processing, Nonlinearity Compensation**

I. Introduction

SIGNAL processing techniques to overcome optical fiber nonlinearity have evolved considerably in recent years. With the aim of increasing the capacity and reach of coherent detection systems, the use of digital signal processing (DSP) algorithms has been shown to significantly improve system performance [1] and reduce complexity [2] when compared to earlier systems. The digital back propagation (DBP) algorithm [3] is conventionally applied at the receiver, however it can also be applied at the transmitter (i.e., digital pre-compensation [4], [5]), or as some combination of both link endpoints, as investigated in [6]. In all cases, DBP seeks to simulate a reverse link (see Fig. 1) and, consequently, reverse the deterministic nonlinear and linear fiber propagation effects [3].

Manuscript received January, 2018. This work was funded by United Kingdom (UK) Engineering and Physical Sciences Research Council (EPSRC) Programme Grant UNLOC (UNLocking the capacity of Optical Communications), EP/J017582/1. D. Lavery is supported by the Royal Academy of Engineering under the Research Fellowships scheme.

*These authors contributed equally to this work. T. Sherborne and B. Banks were students within the Department of Electronic and Electrical Engineering, University College London, London WC1E 7JE, U.K. (e-mail: zceetrs@ucl.ac.uk; zceebjb@ucl.ac.uk).

D. Lavery, D. Semrau and P. Bayvel are with the Optical Networks Group, Department of Electronic and Electrical Engineering, University College London, London WC1E 7JE, U.K. (e-mail: d.lavery@ucl.ac.uk; d.semrau@ucl.ac.uk; p.bayvel@ucl.ac.uk).

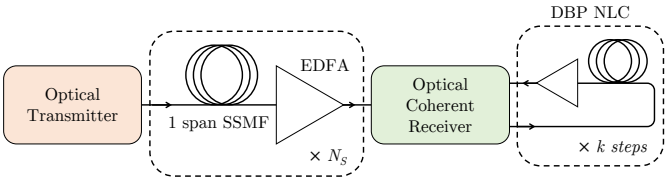

Fig. 1. Transmission model used to investigate the performance of various DBP schemes. This is implemented as a series of linear and nonlinear operators applied to the buffered signal vector. *Ideal* DBP describes the most intensive implementation of DBP with k steps equal to the number of steps applied over N_s spans in simulated forward propagation.

However, the promising performance gains achieved with ideal DBP typically incur a computational expense beyond the capabilities of present digital signal processing hardware [7], due to the use of the split step Fourier method to solve the reverse Nonlinear Schrödinger equation (NLSE) as a Manakov system [8]. In order to achieve real-time processing, several implementations of DBP have been proposed with differing perspectives on the trade-off between performance and complexity. These included increasing the nonlinear step size of the split step Fourier method in the DBP virtual link to minimize the number of calculations required for signal recovery. 1 step-per-span DBP (1sps-DBP) [3] has been proposed as a natural trade-off between performance and complexity for single channel DBP. More advanced proposals include the low pass filter DBP (LPF-DBP) - an implementation of DBP that introduces a phase noise filter in the nonlinear step of the algorithm [9]. High frequency phase noise components are present in the phase spectrum when measured across multiple spans, and the use of LPF-DBP acts to suppress such components to achieve reasonable performance with < 1 step per span. LPF-DBP has been shown to perform comparably to 1sps-DBP with 1 step every 4 spans [9], corresponding to an approximately 75% reduction in the number of calculations required for NLC. Note that the overall numerical complexity of the aforementioned NLC schemes is dependent on the link length.

DBP is typically implemented as a Wiener-Hammerstein system [7] on a 'virtual' link expressing a reverse journey to the physical forward propagation. The conventional Manakov system for modeling propagation concatenates operators of fixed distance to describe the full link, and so the complexity of standard DBP, which uses this approach, is proportional to the link length. A recent development in the field has been the design of low complexity NLC methods with a nonlinear step

size equal to the physical link length [10].

For realizable NLC in a coherent receiver, any solution would ideally demonstrate performance improvement over chromatic dispersion compensation (CDC) while avoiding a significant increase in computational complexity. This has spurred interest in single step-per-link implementations of DBP. The Enhanced Split Step Fourier Method (ESSFM) is a general implementation of filtered DBP, which applies the reversed channel with the step size equal to the link length [10]. Similarly to LPF-DBP, the ESSFM uses an additional operation stage in the nonlinear algorithm sub-step. The ESSFM algorithm has demonstrated a performance increase of 0.7 dB [11] versus linear equalization with a comparable demand of complex multiplications [11]. Both methods of augmented DBP use nonlinear optimization routines for the determination of a nonlinear filter [11], [12]. This routine solves a numerical problem and not the underlying problem of solving an indeterminate equation describing a physical system, and therefore it is uncertain if either method demonstrates optimality in their solutions.

These implementations of DBP have demonstrated the potential performance benefits of using NLC over CDC in offline implementations. However, to make a case for the practical deployment of such systems there remains a question of DBP performance when constrained to the fixed point arithmetic required in a high throughput coherent receiver.

This has previously been investigated in [13], where time domain dispersion filters, with a manually optimized dispersion compensation ratio between the linear filters was used to minimise hardware requirments. To extend the general understanding of quantization effects in NLC methods, here we investigate frequency domain dispersion compensation, similarly making no assumptions on the target hardware. An advantage of the hardware- and system-agnostic approach is that it facilitates a clearer comparison between different NLC methods, where a change in dispersive block length can have a significant impact on performance, while removing the consideration of distortions introduced by finite-length time domain filters [14][1].

Therefore, in this paper, we develop a model of finite precision arithmetic and simulate the operation of several implementations of DBP. We assess and compare the performance of constrained DBP using the linear CDC algorithm as a benchmark. Finally we determine operating regimes for which a specific implementation of NLC outperforms CDC in terms of SNR.

This paper is organized as follows. In Section II-A, different NLC algorithms are introduced. In Section II-B, the model of fixed-point arithmetic and hardware simulation is described in detail. The results of the transmission simulations are given in Section III-A for the DBP fixed point algorithm and Section III-B for the ESSFM fixed point algorithm. Conclusions are drawn in Section IV.

[1]It should be noted that, although the time domain DBP has now seen implementation in ASIC [15], several approaches have been recently developed to specifically tackle this issue and enable practical hardware implementations of time-domain DBP. These include random step size DBP [16], and machine learned CDC filter coefficients [17].

TABLE I
SUMMARY OF SYSTEM PARAMETERS

Parameter	Value	Units
Fiber attenuation	0.2	dB/km
Dispersion parameter	17	ps/(nm · km)
Fiber nonlinear coefficient	1.2	1/(W · km)
Span length	40	km
Number of spans	25	-
1spl-DBP/ESSFM step size	Varies	m
Symbol rate	32	GBd
EDFA noise figure	5	dB
Pulse shape	RRC, 1%	rolloff
DBP Wiener-Hammerstein split	0.85	-
ESSFM Wiener-Hammerstein split	0.4	-

II. METHODOLOGY

A. Numerical Simulations and Algorithm Design

In modeling the behavior of digital NLC we used a simulation model of an optical link (Fig. 1), assuming ideal noise-free transceivers, with the link parameters given in Table I. The signals under test were single channel 32 GBd dual polarization (DP) quadrature phase shift keying (QPSK) and 16-*ary* quadrature amplitude modulation (DP-16QAM) signals. The signal was sampled at 4 samples/symbol and shaped using a root-raise cosine (RRC) filter. In this approach, we numerically solved the Manakov system for forward pulse propagation to simulate 1000 km (25×40 km span) of standard single-mode fiber (SSMF), as a representative long-haul transmission system, and following the methodology in [11]. An EDFA was included after each span to fully compensate for the power loss due to signal attenuation over the span.

Fig. 2 shows the receiver model used in this work. The received data is detected, resampled to 2 samples/symbol and normalized to unit average power. The signal is then processed using either EDC (implemented as a single step frequency domain filter), or the NLC algorithm under test. The approaches to NLC in this work are the ESSFM [10] at 1 step-per-span, and DBP at between 1 and 5 steps-per-link (i.e., up to 1 step-per-span). In the implementation of each NLC algorithm, fixed-point arithmetic is used to model the finite precision available in practical hardware. Details of the fixed point modules are discussed in Section II-B. For both DBP and EDC, the Fast Fourier Transform (FFT) is based on the radix-2 Cooley-Tukey algorithm [18] using an 'overlap and save' procedure to model a buffered application of dispersion compensation. Exponentials were approximated using the coordinate rotation digital computer (CORDIC) algorithm to reduce the computational demand of approximation using a long Taylor series (although note that truncated Taylor series have also been successfully used in, e.g., [13]). The filter coefficients for the ESSFM algorithm were optimised offline using a double precision floating-point non-linear optimization algorithm, and the coefficients were quantized at runtime. Following NLC or EDC, matched filtering was applied to the signal, before normalization and downsampling to 1 sample/symbol. SNR estimation was performed on the central 2^{14} symbols, as per the approach and assumptions in [19] and is reported for the optimum launch power unless otherwise specified.

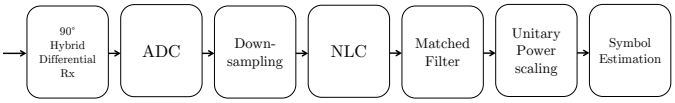

Fig. 2. The signal processing chain used in this work. The complex valued pulse train is captured using a model of balanced detection, downsampled to 2 samples/symbol, NLC applied and match filtered before unitary scaling and an SNR for the symbols estimated. This routine is also the function, $f(x)$, for the optimisation of the ESSFM filter coefficients.

DBP was applied using the split-step Fourier method (SSFM) to solve the Manakov equation [20] with the inverse loss, dispersion and nonlinearity fiber coefficients. The single channel transmission at 32 GBd with 40 km spans was chosen for equitable comparison of algorithm performance between DBP and ESSFM, again, following the methodology of [11]. The Manakov inverse channel model [20], over some incremental step, h, approximates the deterministic effects of the channel as

$$\begin{aligned}\mathbf{E}(z+h,T) &\simeq \exp(h\hat{D})\exp(h\hat{N})\mathbf{E}(z,T) \\ &\simeq \exp\left(\frac{h}{2}\hat{D}_1\right)\exp(L_{\text{eff}}\hat{N})\exp\left(\frac{h}{2}\hat{D}_2\right)\mathbf{E}(z,T),\end{aligned} \tag{1}$$

where $\hat{D}$ is the linear operator, given by

$$\hat{D} = \frac{i\beta_2}{2}\frac{\partial^2}{\partial t^2}, \tag{2}$$

and $\hat{N}$ is the nonlinear operator, defined as

$$\hat{N} = -i\gamma\frac{8}{9}\mathbf{E}^{\mathbf{H}}\mathbf{E} - \frac{\alpha}{2}. \tag{3}$$

Here, $\mathbf{E} = [E_X, E_Y]$ is the optical field in the X and Y polarization states, α is the fiber loss parameter, β_2 is the group velocity dispersion, γ is the fiber nonlinearity coefficient, and L_{eff} is the effective length of h.

Following the approach described in [7], a 3- block Wiener-Hammerstein model for each step was used for the DBP. Linear compensation sub-steps were performed in the frequency domain with a circular convolution using 4 FFTs per step. For DBP, adjacent linear blocks were combined over the total link for $N_s + 1$ total FFT blocks. Nonlinear substeps were applied in the time domain as a phase shift proportional to the instantaneous power of the back propagating signal. The responsibility of application of the linear components between each $\hat{D}_i$ block in (1) is dictated by the Wiener-Hammerstein (WH) split. This parameter has the effect of controlling the position of the nonlinear $\hat{N}$ term across step distance, h.

To implement the ESSFM algorithm proposed in [10], we use a modified nonlinear operator

$$\hat{N}_k = -i\gamma L_{eff}\left(\sum_{i=0}^{N_c} c_i\left(|\mathbf{E_{k-i}}|^2 + |\mathbf{E_{k+i}}|^2\right)\right) \tag{4}$$

for each sample, k, with the application of the ESSFM filter coefficients, c_i, for filter size N_c+1. The filter coefficients are determined through a nonlinear multivariate equation solver. The DSP chain for signal processing, including the ESSFM, is formulated as some function, $f(x)$, which returns a final SNR. In this work, a Quasi-Newton cubic line search procedure was used to minimize a negated SNR output of $f(x)$. This blind optimization approach uses gradient descent with a relative tolerance of 10^{-3} to converge on a set of filter coefficients. Similarly to [11], we applied nonlinear optimization to maximize the SNR of a sample sequence using the coefficients, c_i as the degrees of freedom. The number of coefficients in the filter was restricted to a power of two, again for direct comparison with [11]. The number of multiplications per transmitted symbol for the ESSFM $\hat{N}$ operator can be approximated by $N_s(2N_c + 1)$ when the multiplications for instantaneous power are disregarded[2]. This linear relationship suggests the possibility for an optimality trade-off between ESSFM filter size and performance in SNR. Diminishing returns for the system in [11] were observed for filters of 32 tap weights and above. Here, this investigation was repeated for our system parameters, as it can be seen that additional multiplications in the $\hat{N}$ operator have implications for the performance limitations from the quantization overhead in the fixed point model; there is a trade off between nonlinear performance gain and quantization noise introduced from the additional filter taps. The theoretical basis for the operation of the ESSFM and the filter coefficients is further discussed in [11], [21].

In this paper, we follow the approach taken in [10] and operate the ESSFM at the 1 step-per-link level. In this case the Wiener-Hammerstein (WH) split now determines the position of the only nonlinearity compensation operator across all spans. We confirmed the optimal WH split value of 0.85 for DBP, as expected [7]. However for the ESSFM, the WH split was fully re-optimized. The intuition for this is that since the distribution of power over distance for a step size of 1 span length is only a subset of the distribution over the full link, the location of the single $\hat{N}$ would likely change. In [11] the ESSFM is proposed using the Wiener Model of the $\hat{N}$ term preceding a singular $\hat{D}$ term. We found this arrangement to be sub-optimal in terms of nonlinear compensation performance, despite the additional quantization from two FFT pairs per link, and we subsequently used an optimized WH split value of 0.4.

B. Hardware Model

When implementing NLC algorithms in hardware, the finite precision, fixed-point (FXP), arithmetic will have an impact on the achievable SNR. For the different NLC schemes, it is possible to compare the performance and complexity merits of such algorithms in a practical scenario. To do this, it is necessary to model the bit-level arithmetic occurring in realtime receiver hardware.

A set of software functions to model FXP arithmetic for an arbitrary quantization level were developed. This model

[2]Note that the ESSFM filter is a symmetric FIR filter and this symmetry could be exploited to efficiently implement the FIR filter in hardware.

remains agnostic to the hardware platform, with no intended target system (as in, e.g., [13]). The basis for this model are functional blocks for FXP addition and multiplication, which receive some quantization level as an input parameter and return the arithmetic result. The constraints investigated here are limited to bit depth (the number of logical bits permitted in FXP arithmetic) as a primary factor in the degree of accumulated quantization and the size of the FFT window. Intuitively, a decrease in bit depth leads to greater quantization noise as the bit stream is increasingly compressed. This limits the ability of the FXP model to approximate the best case (64-bit floating point, hereafter 'double precision') simulation model, resulting in some level of performance degradation.

These atomic, arithmetic functions were used to emulate the operation of more complex operations, including an FFT. A fixed bit depth was assumed throughout the system and bit depth expansion was not permitted across multiple functions, as is typical in real-time signal processing hardware. However bit depth expansion is permitted for intermediate operations only[3]. Each number is represented in simulation using the fractional two's complement fixed point format, with each representable value in the range $-1 \leq x < 1$. This format was chosen as there is a guarantee that the product of every multiplication will have some magnitude equal or less than that of either input. The sampling of a continuous signal to some discrete amplitude introduces quantization noise, resulting in error propagation as a result of the finite precision of the system. As a sample propagates through a cascade of multiplication stages (e.g., in the FFT) then each multiplication introduces some quantization noise. The signal-to-quantization noise ratio of a signal quantized to B bits [22] can be described as

$$SQNR = \frac{1}{\sigma^2}, \tag{5}$$

where the quantization noise variance is given by

$$\sigma^2 = \frac{2^{-2B}}{12} \tag{6}$$

The logarithm of Eq. (5) reveals a gain of 6 dB in SQNR for the provision of an extra bit. The crux of Eq. (5) in the context of digital NLC is the trade-off between maximizing the number of DBP steps in order to ensure solution accuracy and minimizing the number of steps to prevent the accumulation of quantization noise.

When an input signal is first quantized to a set bit depth, each amplitude is rounded towards the nearest available discrete amplitude. In the event of an arithmetic overflow in this system, the erroneous value is clipped at maximum or minimum quantized amplitude. (Arithmetic overflow refers to some discrete number outside of the $[-1, 1)$ bounds.) This method also ensures the quantization noise distribution remains zero-centered.

[3]We refer to an intermediate operation as one inside a single function block but between the atomic function units. The primary usage of this intermediate bit expansion is during the FFT block, wherein conditional scaling of bit depth is employed to minimize the addition of quantization noise from successive FXP operations. This problem could also have been approached by choosing a different quantization interval, however in this work the bounds $x \in [-1, 1)$ are strictly enforced.

Within the NLC algorithms, transformations between the time and frequency domain are performed by a radix-2 Cooley-Tukey FFT [18]. This format of FFT is chosen for the ability to implement a wide range of FFT sizes and because the complexity of this FFT is well studied [11]. We did not consider split radix FFTs in this work, which may have changed the overall NLC performance. However, because the same FFT implementation is common to all algorithms considered, any performance change would affect all NLC implementations. The quantization noise introduced from one butterfly operation in an FFT is $4\sigma^2$ with a quantization noise variance introduced from an FFT as $4(N-1)\sigma^2$ [22]. This corresponds to the optimal SNR achievable for a signal processed using an FFT and, as such, places a ceiling on total system performance.

The Overlap and Save algorithm was used to be able to model the continuous filtering required in hardware. The size of the buffer to process must correspond to a radix-2 FFT size, or 2^n, where $n \in \{5, \dots 15\}$. An overlap size of $N/4$ was chosen, where N is the length of a signal buffer, in correspondence with the work carried out in [11]. The Overlap and Save algorithm used here also applies the dispersion map as the linear substeps of DBP and the full CDC operation. Nonlinearity compensation is applied in the time domain by multiplying the signal with a vector of complex exponentials via CORDIC [23].

III. Results

A. Digital Back Propagation

The initial simulations of the transmission of 2^{18} DP-QPSK modulated samples at 32 GBd over a 1000 km fiber link. DBP was implemented with the parameters described in Section II-A with the finite precision logic described in Section II-B. For comparison, we also implemented CDC using the same FXP modeling constraints. The FFT size was optimized in each case and is therefore not included as a parameter. In the following, we examine the behavior of DBP in the FXP environment, and discuss the additional complexity of this form of NLC compared to CDC.

Fig. 3 shows the SNR improvement relative to CDC at the same FXP bit depth, across a range of numbers of nonlinear steps-per-link. For an increased number of steps in DBP, the virtual link model improves in efficacy, as expected, however this is at the cost of an increased FXP bit depth, which is required to reduce the impact of quantization noise when multiple steps are used. Additionally, Fig. 3 identifies that there exists some quantization limit in performance, at a given number of steps-per-link, which can be reached with a sufficient bit depth in the digital logic. In the single step per link case, with the fewest multiplications, there is a negligible SNR gain of 0.1 dB over CDC for bit depths greater than 13 bits. We observe no gain in SNR over CDC for bit depths below this, for any number of steps-per-link. The greatest performance difference over CDC is a ≈3 dB gain, observed using 1 step-per-span, was at a bit depth of 16 bits. However, when compared to a fixed point implementation of CDC, it can be seen that any gain requires a minimum of 13 bits.

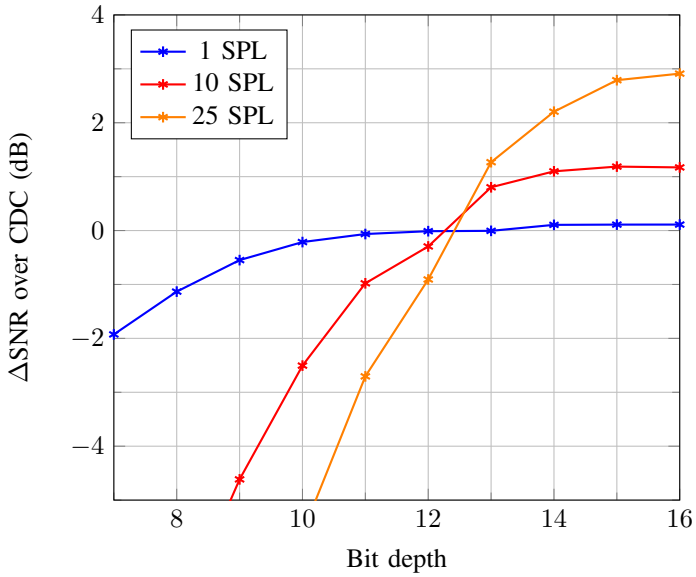

Fig. 3. SNR improvement for DBP compared to CDC at 1000 km for DP-QPSK transmission. Both DBP and CDC are simulated with FXP arithmetic and optimized FFT size. DBP is simulated with a range of steps-per-link (SPL) to investigate the influence of the number of steps on the quantization error on the signal.

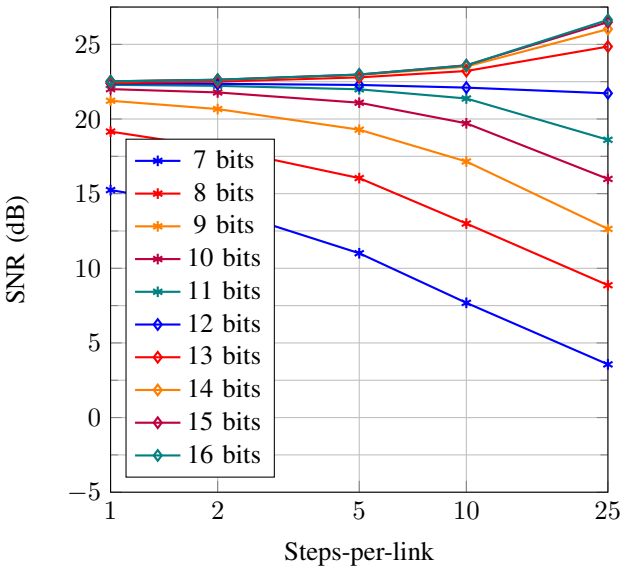

Fig. 4. SNR against the number of steps-per-link for DBP at 1000 km for 32 GBd DP-QPSK transmission. DBP is simulated with FXP arithmetic with the number of steps in the virtual fiber model and bit depth varied. Note that 15- and 16-bit FXP performance at 25 steps-per-link is within 0.1 dB of double precision floating point.

We expand on this analysis in Fig. 4 by examining the absolute SNR performance of DBP against the variation in steps-per-link between 7 and 16 bits. From this result it can be inferred that for ≤ 12 bits, there is insufficient arithmetic precision to tolerate the increased accumulation of quantization noise arising from increasing the number of DBP steps-per-link. While increasing the steps-per-link increases the accuracy of theoretical DBP our results show that increasing the number of FFTs and multiplications is monotonically detrimental for low bit depths due to quantization error. However for ≥ 13 bits, there is a noted transition to an operating regime for which an increase in the steps-per-link results in some SNR gain. This confirms that at 1000 km, a minimum of 13 bits are required to overcome the quantization overhead present in our implementation of DBP. Notably, for a resolution of 10 bits, the SNR intially increases, and then decreases beyond 2 steps-per-link; i.e., there exists an *optimum* number of steps-per-link for a given FXP hardware bit depth. Previously reported results in this area show that DBP performance increases monotonically with number of steps-per-link and, thus, this result highlights the importance of considering fixed point arithmetic in performance analyses.

To conclude this section, we now consider the optimised FFT transform window used for each data point in Fig. 4. Shown in Fig. 5 is the average FFT transform window used for each bit depth. We note that the trend is approximately linear when considering the number of butterfly stages (i.e., the binary logarithm of the number of samples). Between bit depths of 8 and 15, the transform size doubles for each increment in bit depth; as expected from theory. For the highest bit depths, we did not see any benefit for increasing the transform window beyond 2^{15}, hence the saturation at this point.

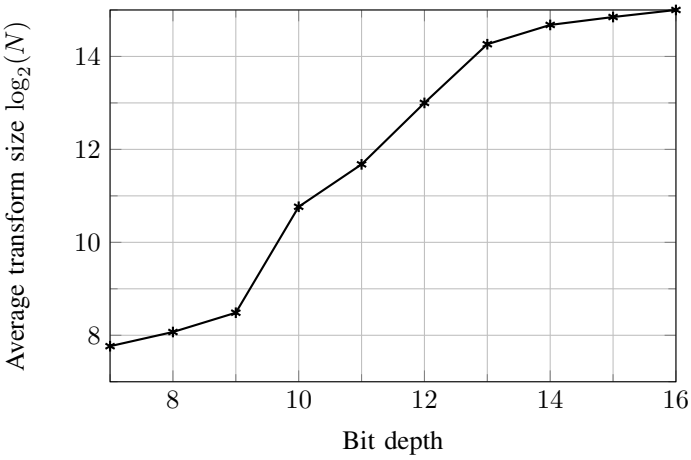

Fig. 5. The FFT transform size which maximises the SNR, averaged across all the data presented in Fig. 4. Note that the maximum transform size was set to 2^{15}, as this was sufficient to match the double precision performance at high bit depths.

B. Enhanced Split Step Fourier Method

The ESSFM algorithm described in Section II-A was simulated in the system detailed by Fig. 2. For the DP-QPSK scenario, Fig. 6 identifies the variation in SNR against launch power. Each power and coefficient filter size was separately optimized up to a filter of size $N_c = 256$.

Improvements in SNR compared to CDC were observed for all input powers near the optimum. The maximum SNR improvement was 0.7 dB for DP-QPSK and 0.8 dB for DP-

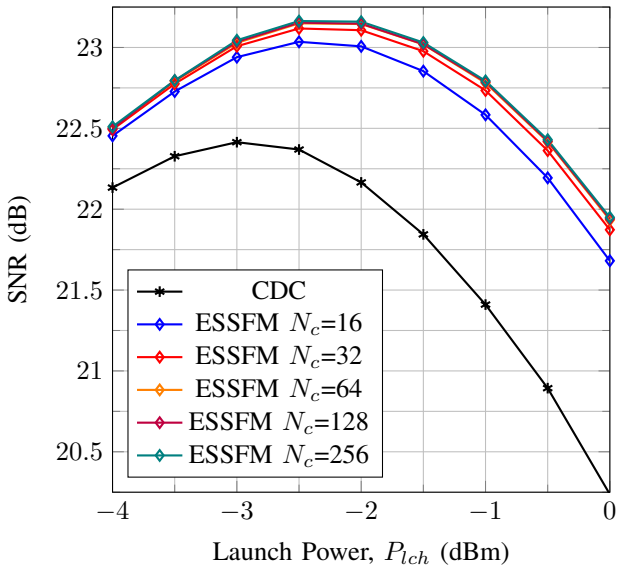

Fig. 6. SNR against launch power for the ESSFM applied as NLC to a 32 GBd DP-QPSK signal. The CDC baseline is also shown. This simulation was produced using double-precision floating point arithmetic, representing the ceiling of achievable performance for a comparable fixed point simulation which will have a non-negligible quantization penalty.

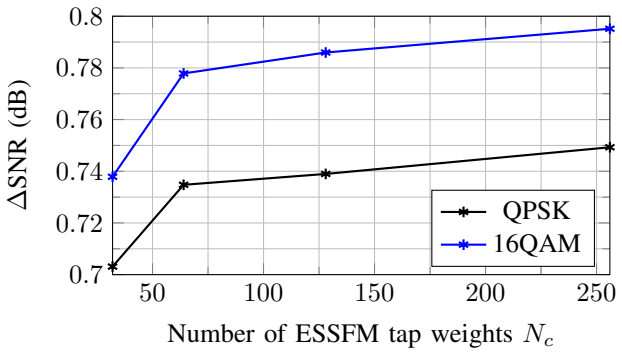

Fig. 7. ΔSNR over CDC for the ESSFM at optimum P_{lch} for increasing filter size.

16QAM with a 256-tap filter (cf. the original results for this algorithm as presented in [11]). Fig. 7 shows the trade-off between filter size and NLC performance, indicating that $N_c = 128$ represents a good trade-off between performance and complexity. This filter length is therefore used for the remainder of this work.

Previous research into modifying the nonlinear operator in DBP [11], [12], [24] used a black box approach generating an optimal filter. We follow this methodology, however we chose to inspect further the behavior of the filter returned through the optimization routine detailed in Section II-A. In Fig. 8, the 128-tap filter for processing a DP-QPSK signal at the optimum launch power is analyzed in the frequency domain. The profile of this filter is effectively a weighting of a neighboring samples' power to each sample. Fig. 8 demonstrates that this filter exhibits a low pass filtering behavior that was not a constraint intended as part of the design. We note that this highlights more similarity between the methods of the LPF-DBP and the ESSFM, as the coefficients in the ESSFM were not originally proposed as a filter of any specific kind. With the understanding that the $\check{N}$ operator in the ESSFM is performing a linear phase[4] low pass filtering with one NLC term per link. We suggest that, for future work, it may be sufficient to combine the approaches of [24] and [11] (i.e., through the direct optimization of the filter bandwidth within the ESSFM), which was essentially the approach taken in [9].

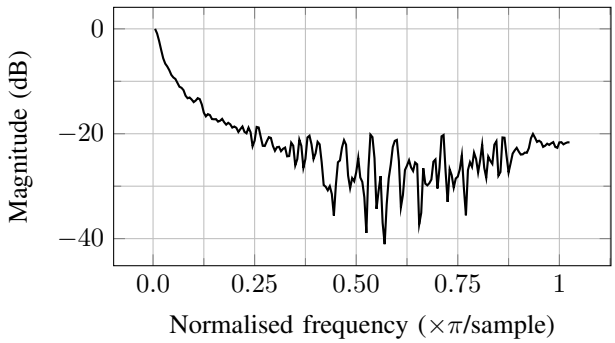

Fig. 8. Frequency response of the 128-tap ESSFM $\check{N}$ operator for 32 GBd DP-QPSK transmission.

Finally, the behavior of the ESSFM as NLC in a finite precision arithmetic simulation is explored. Fig. 9 shows the maximum SNR improvement over FXP CDC with a varying number of bits and FFT size optimized for each bit depth. It can be seen that, as anticipated, there exists some quantization penalty limiting the finite precision algorithm performance when compared to double precision. The difference between the overheads of 0.024 dB for DP-QPSK and 0.18 dB for DP-16QAM highlights a potential level of increased sensitivity to quantization for multi-level modulation formats. As the level of quantization noise is constant for any distance with the ESSFM, there exists some link length at which channel noise dominates over quantization noise and this overhead becomes negligible. The exact location of this crossover point was not explored, as it is an inherently system-dependent parameter, however it is estimated from preliminary results to be near a link length of 2000 km for the system considered herein.

The results in Fig. 9 also highlight the limitations of even low complexity DBP when compared to CDC, as a minimum of 10 bits are required to improve over linear equalization. Indeed, the relatively high bit depth requirements shown are as a result of the use of frequency domain CDC, and the hardware requirements have been shown to be correspondingly lower for time domain algorithms [13]. For the present work, though, it is the relative performance (rather than absolute performance) of the algorithms which is of primary interest. Comparing

[4]The linear phase response of the ESSFM 128-tap filter is not shown in this work for brevity. Also not shown is similar low pass behavior for the 128-tap filter designed for DP-16QAM.

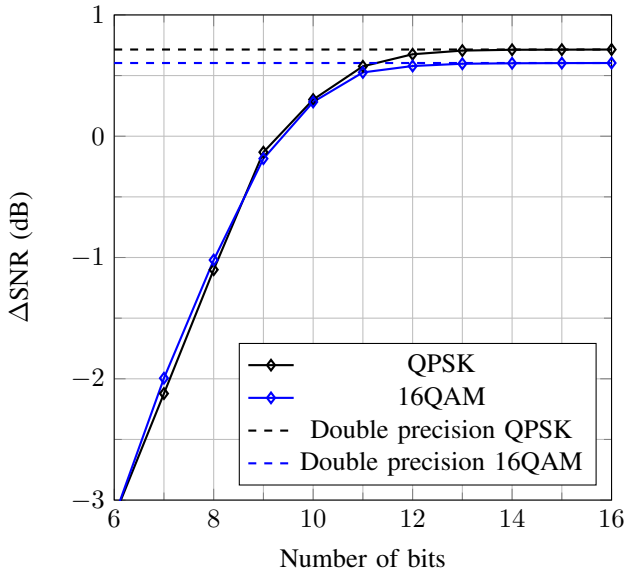

Fig. 9. ΔSNR over CDC for the ESSFM against bit depth at 1000 km for 32 GBd DP-QPSK and DP-16QAM transmission. The double precision performance is shown for reference.

Fig. 3 and Fig. 9, we observe that, at a 1 step-per-link level, the low complexity ESSFM demonstrates improvements in SNR performance when compared to both DBP and EDC. However, this gain in SNR remains less than 1 dB and is sub-optimal when compared to a DBP using a greater number of steps-per-link. Provided there is a sufficient number of bits to saturate the system performance, Fig. 3 demonstrates that more steps-per-link will yield greater SNR improvement compared to the addition of the nonlinear phase filter in the ESSFM. Nevertheless, it should be noted that the ESSFM outperforms DBP for all bit depths $\leq$13 bits, irrespective of the number of steps used for DBP. It is anticipated, based on recently reported results [13], that when using time domain CDC as part of the NLC algorithms, that this difference in bit depth requirements would persist, albeit at a low required number of bits for both DBP and ESSFM.

IV. Conclusion

The behavior of algorithms for optical fiber nonlinearity compensation were investigated in detail under the constraint of fixed-point arithmetic. Using a simulation including an ideal transmitter and coherent receiver, limitations on performance for signal recovery in DSP, have been shown, and are primarily a result of quantization noise. It was found that, for this frequency domanin NLC implementation, a minimum of 13 bits is required to observe any additional SNR gain from $\geq$ 1 step-per-link DBP. A similar bit depth is required to reach the maximum achievable performance benefit over CDC for the ESSFM algorithm, however we note that some improvement over CDC can be seen with the reduced constraint of 10 bits. Although other algorithms for simplified DBP exist [25], [26], the work presented herein has shown that it is crucial to include an analysis of bit depth in order to accurately compare the performance of different NLC algorithms, and that the number of mathematical operations, alone, cannot serve as a proxy for complexity. Even with reductions in complexity achieved using time-domain DBP [13] (which showed requirements of approximately 8-10 bits for two steps-per-span DBP) the differences in requirements between DBP and ESSFM would persist.

We also highlight, for the first time, the similarities in behavior of the ESSFM and LPF-DBP through the observation that the frequency response of the ESSFM phase filter exhibits low pass filtering behavior. Future work on this topic could include the investigation into the behavior of the aforementioned NLC in a multi-channel or super-channel system, as well as expanding on the impact of modulation format on the quantization penalty of the finite-precision ESSFM.

More generally, we note that the fixed point models developed herein could be used as a basis for estimating the true performance of any NLC algorithm, and should, therefore, be included as inherent consideration in the NLC algorithm design process.

Acknowledgment

The authors wish to extend their thanks to Drs Rachid Bouziane and Philip Watts, for enlightening discussions on the topic of hardware design, and assistance with developing the models used in this work. The authors are also grateful to the reviewers, particularly for their attention to detail when providing comments on this manuscript.

References

[1] P. Bayvel, C. Behrens, and D. S. Millar, "Chapter 5 - Digital Signal Processing (DSP) and its application in optical communication systems," in *Optical Fiber Telecommunications (Sixth Edition)*, 6th ed., ser. Optics and Photonics. Boston: Academic Press, 2013, pp. 163–219.

[2] A. Napoli, Z. Maalej, V. A. J. M. Sleiffer, M. Kuschnerov, D. Rafique, E. Timmers, B. Spinnler, T. Rahman, L. D. Coelho, and N. Hanik, "Reduced complexity digital back-propagation methods for optical communication systems," *Journal of Lightwave Technology*, vol. 32, no. 7, pp. 1351–1362, 2014.

[3] E. Ip and J. M. Kahn, "Compensation of dispersion and nonlinear impairments using digital backpropagation," *Journal of Lightwave Technology*, vol. 26, no. 20, pp. 3416–3425, 2008.

[4] E. Temprana, E. Myslivets, L. Liu, V. Ataie, A. Wiberg, B. Kuo, N. Alic, and S. Radic, "Two-fold transmission reach enhancement enabled by transmitter-side digital backpropagation and optical frequency comb-derived information carriers," *Opt. Express*, vol. 23, no. 16, pp. 20 774–20 783, Aug 2015.

[5] K. Roberts, L. Chuandong, L. Strawczynski, M. O'Sullivan, I. Hardcastle, "Electronic precompensation of optical nonlinearity," *IEEE Photon. Technol. Lett.*, vol. 18, no. 2, pp. 403–405, Jan. 2006.

[6] D. Lavery, D. Ives, G. Liga, A. Alvarado, S. J. Savory, and P. Bayvel, "The Benefit of Split Nonlinearity Compensation for Single-Channel Optical Fiber Communications," *IEEE Photonics Technology Letters*, vol. 28, no. 17, pp. 1803–1806, 2016.

[7] D. S. Millar, S. Makovejs, C. Behrens, S. Hellerbrand, R. I. Killey, P. Bayvel, and S. J. Savory, "Mitigation of fiber nonlinearity using a digital coherent receiver," *IEEE Journal on Selected Topics in Quantum Electronics*, vol. 16, no. 5, pp. 1217–1226, 2010.

[8] G. P. Agrawal, *Applications of Nonlinear Fiber Optics (2nd Edition)*, 2nd ed. Elsevier, 2008.

[9] L. B. Du and A. J. Lowery, "Improved single channel backpropagation for intra-channel fiber nonlinearity compensation in long-haul optical communication systems." *Optics express*, vol. 18, no. 16, pp. 17 075–17 088, 2010.

[10] M. Secondini, D. Marsella, and E. Forestieri, "Enhanced split-step Fourier method for digital backpropagation," *European Conference on Optical Communication, ECOC*, no. 1, pp. 3–5, 2014.

[11] M. Secondini, S. Rommel, G. Meloni, F. Fresi, E. Forestieri, and L. Potì, "Single-step digital backpropagation for nonlinearity mitigation," *Photonic Network Communications*, vol. 31, no. 3, pp. 493–502, 2016.
[12] Y. Gao, J. H. Ke, J. C. Cartledge, and S. Yam, "Low-Pass Filter Assisted Digital Back Propagation Algorithm for 112 Gb/s DP 16-QAM," *Paper SPT5D.5 in Proc. Signal Processing in Photonic Communications (SPPCom) 2013*.
[13] C. Fougstedt, M. Mazur, L. Svensson, H. eliasson, M. Karlsson, and P. Larsson-Edefors, "Time-domain digital back propagation: Algorithm and finite-precision implementation aspects," in *Optical Fiber Communication Conference*. Optical Society of America, 2017, p. W1G.4.
[14] S. J. Savory, "Digital filters for coherent optical receivers," *Optics Express*, vol. 16, no. 2, 2008.
[15] C. Fougstedt, L. Svensson, M. Mazur, M. Karlsson and P. Larsson-Edefors, "ASIC Implementation of Time-Domain Digital Back Propagation for Coherent Receivers," in *IEEE Photonics Technology Letters*, vol. 30, no. 13, pp. 1179-1182, 2018.
[16] C. S. Martins *et al.*, "Efficient Time-Domain DBP using Random Step-Size and Multi-Band Quantization," in *Optical Fiber Communication Conference*. Optical Society of America, 2018, p. W3A.5.
[17] C. Häger and H. D. Pfister, "Deep Learning of the Nonlinear Schrdinger Equation in Fiber-Optic Communications," in Proc. IEEE International Symposium on Information Theory (ISIT), 2018.
[18] J. W. Cooley and J. W. Tukey, "An algorithm for the machine calculation of complex fourier series," *Mathematics of Computation*, vol. 19, no. 90, 1965.
[19] A. Alvarado, E. Agrell, D. Lavery, R. Maher, and P. Bayvel, "Replacing the soft-decision FEC limit paradigm in the design of optical communication systems," *Journal of Lightwave Technology*, vol. 33, no. 20, pp. 4338–4352, Oct 2015.
[20] D. Marcuse, C. R. Menyuk, and P. K. A. Wai, "Application of the Manakov-PMD equation to studies of signal propagation in optical fibers with randomly varying birefringence," *Journal of Lightwave Technology*, vol. 15, no. 9, pp. 1735–1745, 1997.
[21] M. Secondini and E. Forestieri, "On XPM mitigation in WDM fiber-optic systems," *IEEE Photonics Technology Letters*, vol. 26, no. 22, pp. 2252–2255, 2014.
[22] J. G. Proakis and D. G. Manolakis, *Digital Signal Processing*, 4th ed. Pearson Education International, 2007.
[23] S. A. Khan, *Digital Design of Signal Processing Systems: A Practical Approach*. John Wiley & Sons, Ltd, 2011.
[24] Y. Gao, J. H. Ke, J. C. Cartledge, and S. S. H. Yam, "Method for determining the low-pass filter bandwidth for the low-pass filter assisted digital back propagation algorithm," in *39th European Conference and Exhibition on Optical Communication (ECOC 2013)*, Sept 2013, pp. 1–3.
[25] R. Asif, C. Y. Lin, M. Holtmannspoetter, and B. Schmauss, "Logarithmic step-size based digital backward propagation in N-channel 112Gbit/s/ch DP-QPSK transmission," in *2011 13th International Conference on Transparent Optical Networks*, June 2011, pp. 1–4.
[26] C. Häger and H. D. Pfister, "Nonlinear interference mitigation via deep neural networks," in *Optical Fiber Communication Conference*. Optical Society of America, 2018, p. W3A.4.